 doi:10.20944/preprints202102.0093.v1

Article

Planetary Wave Spectrum in the Stratosphere–Mesosphere during Sudden Stratospheric Warming 2018

Yuke Wang [1], Gennadi Milinevsky [1,2,3,*], Oleksandr Evtushevsky [2], Andrew Klekociuk [4,5], Wei Han [1], Asen Grytsai [2], Oleksandr Antyufeyev [6], Yu Shi [1], Oksana Ivaniha [3], and Valerii Shulga [1,6]

1 International Center of Future Science, College of Physics, Jilin University, Changchun 130012, China; wangyk16@mails.jlu.edu.cn (Y.W.); gmilin@univ.kiev.ua (G.M.); whan@jlu.edu.cn (W.H.); shiyu18@mails.jlu.edu.cn (Y.S.); shulga@rian.kharkov.ua (V.S.)
2 Physics Faculty, Taras Shevchenko National University of Kyiv, 01601 Kyiv, Ukraine; evtush@univ.kiev.ua (O.E.); assen@univ.kiev.ua (A.G.); OksanaIvaniha@univ.net.ua (O.I.)
3 Department of Atmosphere Physics and Geospace, National Antarctic Scientific Center, 01601 Kyiv, Ukraine
4 Antarctic Climate Program, Australian Antarctic Division, Kingston 7050, Australia; Andrew.Klekociuk@awe.gov.au (A.K.)
5 Department of Physics, University of Adelaide, Adelaide 5005, Australia
6 Department of Millimeter Radio Astronomy, Institute of Radio Astronomy, National Academy of Sciences of Ukraine, 61002 Kharkiv, Ukraine; antyuf@rian.kharkov.ua (O.A.)

* Correspondence: gmilin@univ.kiev.ua; genmilinevsky@gmail.com; Tel.: +38-050-3525498

Abstract: The planetary wave activity in the stratosphere–mesosphere during the Arctic major Sudden Stratospheric Warming (SSW) in February 2018 is discussed on the basis of the microwave radiometer (MWR) measurements of carbon monoxide (CO) above Kharkiv, Ukraine (50.0° N, 36.3° E) and the Aura Microwave Limb Sounder (MLS) measurements of CO, temperature and geopotential heights. From the MLS data, eastward and westward migrations of wave 1/wave 2 spectral components were differentiated, to which less attention was paid in previous studies. Abrupt changes in zonal wave spectra occur with the zonal wind reversal near 10 February 2018. Eastward wave 1 and wave 2, observed before the SSW onset, disappear during the SSW event, when westward wave 1 becomes dominant. Wavelet power spectra of mesospheric CO variations show statistically significant periods in a band of 20–30 days using both MWR and MLS data. Approximately 10-day periods appear only after the SSW onset. Since the propagation of upward planetary waves is limited in the easterly zonal flow in the stratosphere after the zonal wind reversal during SSW, forced planetary waves in the mid-latitude mesosphere may exist due to the instability of the zonal flow.

Keywords: planetary wave; mesosphere; stratosphere; major sudden stratospheric warming; microwave radiometer; carbon monoxide; wavelet power spectra

1. Introduction

The dynamics of the high-latitude stratosphere in winter is determined mainly by the polar vortex [1,2]. The polar vortex is a stable cyclonic structure that provides western transfer and blocks air mixing in the meridional direction during polar winter [3]. The vertical structure of the polar vortex determines the propagation of the planetary waves (Rossby waves) that penetrate into the middle atmosphere from the troposphere [4–8]. At high activity of planetary waves, the polar vortex is weakening or even change the zonal wind direction from westerly to easterly, when sudden stratospheric warming (SSW) event is observed [9–14] and the destruction of the vortex is accompanied by a sharp increasing of the polar stratosphere–mesosphere temperature [1,15–17].

In the Arctic, sudden stratospheric warming is recorded regularly, occurring approximately every other winter [17], and in some periods even more often [18]. In Antarctica, the vortex is more stable, and two sudden stratospheric warming events have so

Preprints (www.preprints.org) | NOT PEER-REVIEWED | Posted: 2 February 2021 doi:10.20944/preprints202102.0093.v1

far been reported in which the wind direction changed to the opposite at 10 hPa and the stratospheric temperature rose sharply at that altitude. These two events were recorded in September 2002 [16,19,20] and in September 2019 [21,22].

The vertical propagation of planetary waves is realized under conditions of moderate westerly wind in the stratosphere [4,5,8]. Dissipation of planetary waves in the winter stratosphere warms the polar vortex and reduces its strength [7]. In vertical extent, the waves propagate into the mesosphere, where they break, and also weaken the westerlies [23].

Conditions of vertical wave propagation are more favorable for waves with small zonal wave numbers m [4]. So, the main role in the dynamics of the winter stratosphere and mesosphere is played by zonal waves with $m = 1$ (wave 1) and $m = 2$ (wave 2) [8].

The main goal of this paper is to investigate a planetary wave spectrum in the SSW 2018. We study the planetary wave manifestations in the stratosphere and the mesosphere over the Kharkiv region in order to continue analysis of the mesospheric carbon monoxide from the microwave radiometer measurements in Kharkiv [12]. In Section 2, the data and methods of spectral and wavelet analysis of the data are described. In Section 3, the effects of zonal wind reversal during the SSW in zonal anomaly migration are presented, followed by the wave spectrum analysis. The discussion is presented in Section 4 with conclusions in Section 5.

2. Materials and Methods

A high-sensitivity microwave radiometer (MWR), installed in Kharkiv in 2015 and designed to continuously monitor carbon monoxide (CO) profiles, were used in winter–spring season 2018 for observation of the SSW effects. For the measurements technique and the results, see e.g. [12,24]. To analyze quantitatively the planetary waves at different pressure levels in the stratosphere and mesosphere, we used the MWR CO data and data on temperature, geopotential heights (GPH) and CO from the Microwave Limb Sounder on the Aura satellite (Aura MLS) [25–28]. Using the Version 4.2 geopotential height (GPH) data of Aura MLS, the zonal mean zonal wind U has been calculated according to the method of Fleming et al. [29]. The grid of GPH data for calculating U was taken with a step of 2° in latitude. If there is a null value, we use one-dimensional interpolation method to obtain the value of this point.

The quality of the data was checked according to [27]. For each day, data were used for satellite transitions in motion from the ascending and descending nodes of the orbit at pressure levels between 38 hPa and 0.01 hPa. To obtain data, a grid with a step of 1° in latitude and 1.5° in longitude was used. Then, a two-dimensional data set of corresponding longitude and time was formed for each pressure level and orbit direction at values averaged in the latitudinal range from 47.5° N to 52.5° N (around the latitude of Kharkiv). Next, a two-dimensional Fourier analysis was performed for each data set at regular intervals. This analysis allowed obtaining the periods of waves with zonal wave numbers m = 1–5, moving to the east or west, as well as the period of change of the stationary wave.

In the case of the MLS CO data wavelet analysis, the optimal choice of longitude range for analysis is important. If we take ±2.5° around the desired targeted point, then half (~44 days) are missing values (NaN). With the extension of the interval, the number of passes decreases: 34 days at ±3°, 29 days at ±4°, 17 days at ±5°, 11 days at ±5.5°, 7 days at ±5.7°, 1 day at ±6°. For further work, the interval ±5.5° was chosen, which gives a cell with a range of 47.5–52.5° N and 30.5°–41.5° E for the Kharkiv region. Zero values were replaced by averaged values by interpolation. Using the method described by Torrence and Compo [30], wavelet analysis on the MLS and MWR CO data was performed. The Morlet wavelet as wavelet basis function has been chosen. Wavelet transform with the mother wavelet $\psi(t) = e^{-t^2/2} \cdot e^{i \cdot 6t}$ was used.

Preprints (www.preprints.org) | NOT PEER-REVIEWED | Posted: 2 February 2021 doi:10.20944/preprints202102.0093.v1

We then formed a 2-dimensional array of longitude versus time data for each pressure level and orbital direction for values averaged over the latitude range 47.5° N to 52.5° N (within ~2.5° of latitude of Kharkiv). Two-dimensional Fourier analysis was then performed on the each data array for specific time intervals. This analysis yielded the period of eastward and westward propagating waves of wavenumbers m = 1–5 and the period of stationary wave 0.

In this paper we used the MLS data that cover the main phases of the sudden stratospheric warming (SSW) event in 2018 from January 1 up to March 31.

3. Results

3.1. Zonal wave migrations

According to the Charney–Drazin criterion [4], large-scale planetary waves propagate from the troposphere into the stratosphere under the moderate westerly zonal flow condition. As seen from Fig. 1, zonal wind undergoes strong transformation between the pre-warming and warming periods of the SSW 2018. At the Kharkiv latitude 50° N (vertical line), zonal wind of about 30 ms^{-1} takes the height range 40–60 km in January–early February 2018 (Fig. 1a–1b). This wind speed provides propagation of the eastward traveling waves as shown below.

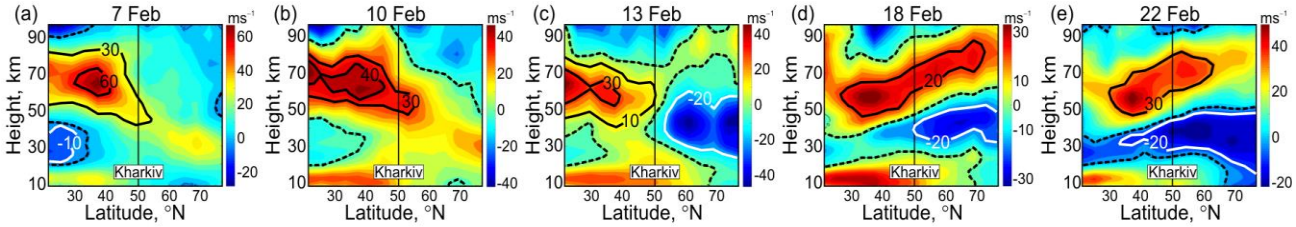

Figure 1. Meridional (latitude–height) cross sections of zonal mean zonal wind on 7, 10. 13, 18 and 22 February 2018 from Aura MLS data [28]. Dashed line shows zero wind. Solid black and white contours outline westerly and easterly zonal flows, respectively, at several characteristic velocities. Vertical line indicated the Kharkiv latitude 50° N.

Layered wind structure appears during the SSW: wind reverses to the easterly in the stratosphere, whereas the westerly maximum 20–30 ms^{-1} is displaced upward into the mesosphere (60–80 km, Fig. 1c–1e; see also [12] for zonal wind reversal in the SSW 2018). Stratospheric zonal wind becomes not favorable for upward wave propagation.

This is seen from the time–longitude variations in the MLS geopotential height (Z) anomalies determined with respect to the mean climatology 2005–2017 for the Kharkiv zone 47.5–52.5° N (Fig. 2). The mesospheric and stratospheric levels during January–March 2018 (Fig. 3a–3e) are presented. Eastward migrating high Z anomalies are observed in the pre-warming period (black dashed lines in Fig. 2) indicating the traveling planetary wave presence under conditions of westerly zonal wind (Fig. 1a and 1b).

Sharp change in the direction of the anomaly migrations from eastward to westward (black and white dashed lines, respectively) around 10 February is clearly seen (Fig. 2). This change coincides with the reversal of the stratospheric westerly to easterly at the Kharkiv latitude at the SSW onset (Fig. 1c–1e). Corresponding change occurs in conditions for propagation of the traveling planetary waves (Fig. 2) in agreement with the Charney–Drazin criterion [4]. Eastward migration in Fig. 2 disappears during the warming and post-warming periods, however westward migration is more distinct in the stratopause–mesosphere region during the SSW event (Fig. 2a–2c). It is seen also that slowly westward migrating anomalies existed in the stratosphere–stratopause altitudes in the pre-warming period (white dashed lines until 10 February in Fig. 2c–2e). This type

Preprints (www.preprints.org) | NOT PEER-REVIEWED | Posted: 2 February 2021 doi:10.20944/preprints202102.0093.v1

of anomalies can be a manifestation of a quasi-stationary planetary wave in the stratosphere.

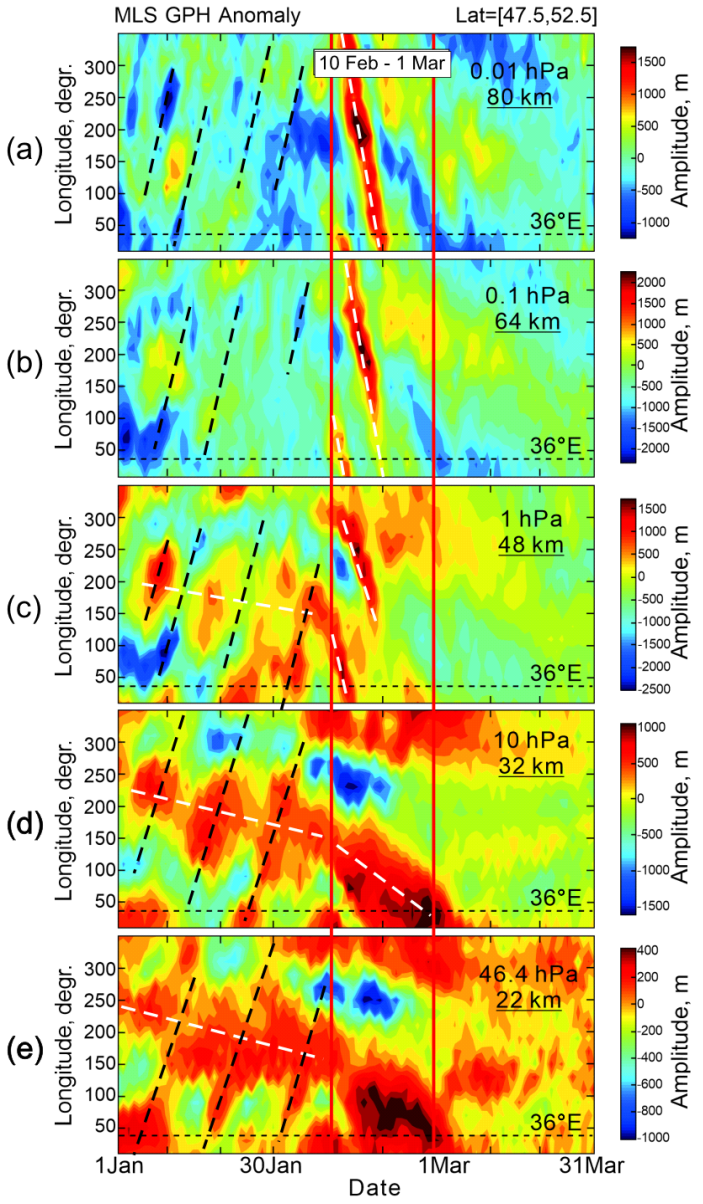

Figure 2. Time–longitude variations of the MLS geopotential height anomalies in the Kharkiv zone 47.5–52.5° N during January–March 2018 with respect to the mean climatology 2005–2017. Red vertical lines mark the SSW event between 10 February and 1 March. Dashed lines indicate eastward (black) and westward (white) high geopotential height anomaly propagation. Dotted horizontal line shows longitude of the Kharkiv station 36° E.

The westerlies in the pre-warming period (Fig. 1a and 1b) provide propagation of the zonal wave 1 and wave 2 with maximum amplitude (derived from the MLS geopotential height) in the stratosphere–lower mesosphere (January–until about 10 February, Fig. 3). The stratospheric easterly since mid-February (Fig. 1d–1e) inhibits upward-propagating planetary waves, as confirmed by change in the wave 1 wave 2 amplitudes (Fig. 3). Wave 2 disappears during the SSW event and later (Fig. 3b). However, gradually weakening wave 1 is observed at 60–80 km (Fig. 3a), at the heights of the westerly maximum (Fig. 1d–1e, see Section 3.2 for explanation).

Preprints (www.preprints.org) | NOT PEER-REVIEWED | Posted: 2 February 2021 doi:10.20944/preprints202102.0093.v1

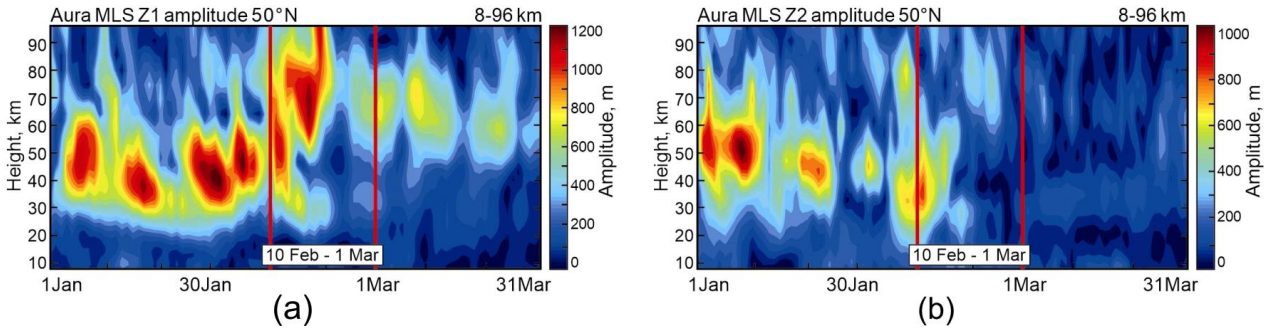

Figure 3. Time–altitude section of (**a**) wave 1 and (**b**) wave 2 amplitude in geopotential height at 50° N in January–March 2018 from the MLS data [28]. Vertical lines mark the SSW event between 10 February and 1 March.

Figures 1–3 demonstrate a close relationship between changes in (i) the direction of the zonal wind associated with the SSW, (ii) the migration of zonal anomalies caused by traveling planetary waves, and (iii) the amplitudes of zonal wave 1 and wave 2. The effect of the Charney–Drazin criterion [4] on the upward propagation of planetary waves is clearly visible.

3.2. Wave spectrum changes

As expected from Figs. 2 and 3, the wave spectrum should change with the zonal wind reversal. In the lower–middle stratosphere, change in the anomaly migration direction (Fig. 2d and 2e) is not as pronounced as at the upper levels (Fig. 2a–2c). Therefore, stratospheric levels were considered for the pre-warming period January–mid-February 2018 using the MLS zonal temperature analysis (Fig. 4). In this period, westerly zonal wind (Fig. 1a and 1b) is favorable for propagation of wave 1 and wave 2 into the stratosphere–lower mesosphere (Fig. 3). Slowly westward migrating positive anomaly in the eastern longitudes is a wave-1 ridge of the quasi-stationary planetary wave (black–white dashed line in Fig. 4a–4c), which dominates in the lower stratosphere (23 km, Fig. 4c). Note that the Kharkiv longitude 36°E (dotted line in Fig. 2 and Fig. 4a–4c) is out of the wave 1 ridge and close to the wave 1 trough during January–March. Wave 1 ridge weakens with altitude and wave 1 trough becomes deeper in the western middle stratosphere (31 km, Fig. 4a).

The vertical wave transformation is accompanied by westward tilt with altitude seen from sequential westward shift of wave 1 ridge and trough in Fig. 4a–4b. By the time of the SSW onset (red vertical line on 10 February, Fig. 4a–4c) the wave 1 ridge in the middle stratosphere approaches the longitude of Kharkiv (31 km, Fig. 4a). At this altitude, the wave 1 ridge is shifted by ~50° to the west relatively its longitudinal position in the lower stratosphere (23 km, Fig. 4c). The westward phase tilt is consistent with upward propagation of the stationary planetary waves (Matsuno, 1970) and supports the identification of the sequence of positive temperature anomalies (black–white line in Fig. 4a–4c) as the ridge of quasi-stationary wave 1.

It is seen that short periods <5 days are not statistically significant in the stratosphere (Fig. 4d–4i). Eastward wave 1 (black dashed line in Fig. 4a–4c) exhibits maximum variance at 10–30 day periods (red curve in Fig. 4d–4f and spectral peaks at $m = 1$ in Fig. 4g–4i). Westward wave 1 and eastward wave 2 (black and blue curves in Fig. 4d–4f) do not show clear periodicity peak; they tend to be more intense at the longest periods (see also $m = -1$ and $m = 2$ in Fig. 4g–4i), i.e. to be quasi-stationary, as was identified above for $m = -1$.

Preprints (www.preprints.org) | NOT PEER-REVIEWED | Posted: 2 February 2021 doi:10.20944/preprints202102.0093.v1

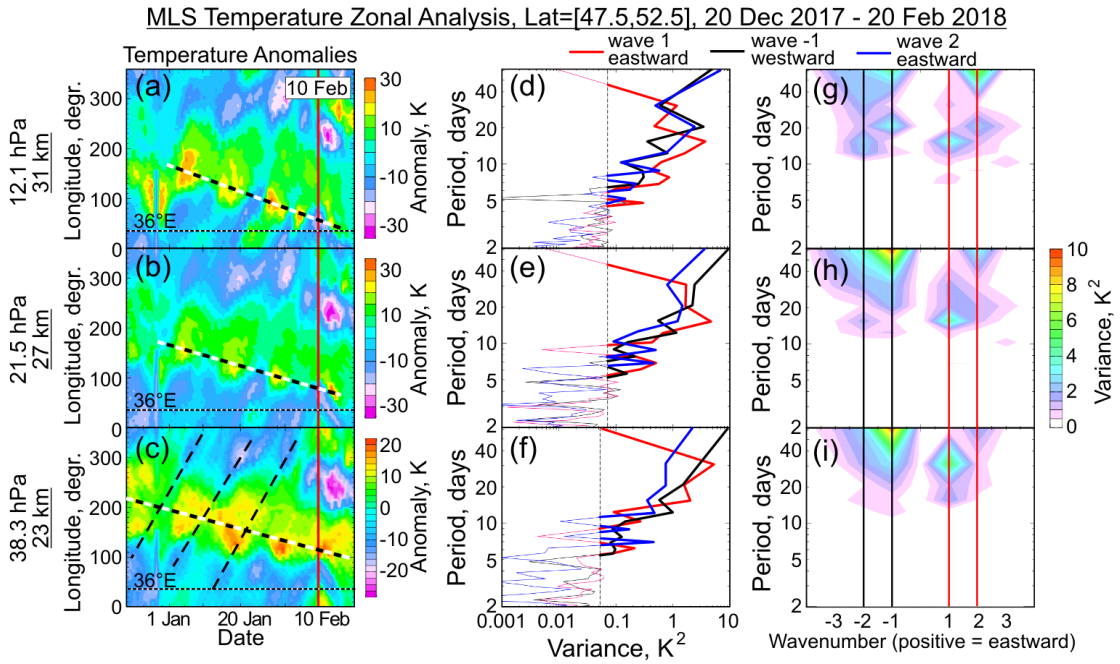

Figure 4. (**a**)–(**c**) As in Fig. 2, but for the zonal MLS temperature anomalies in the lower–middle stratosphere at 23, 27 and 31 km during 20 December 2017 – 20 February 2018; black (black–white) dashed lines indicate eastward traveling wave 1 (quasi-stationary wave, slowly migrating westward); (**d**)–(**f**) wave 1 and wave 2 periods versus variance and (**g**)–(**i**) wave number spectra for the corresponding altitudes; only variances that are statistically significant at the 95% confidence limit are presented. Dashed line in (**d**)–(**f**) marks the 95% confidence limit and bold curves highlight the wave number variance exceeding this limit.

To examine the wave spectrum change in the upper stratosphere–mesosphere before and after the SSW 2018 onset (that is suggested from Figs. 2 and 3), the two 40-day time intervals are compared in Fig. 5. These are 20 December–10 February and 10 February–31 March for the pre- and post-warming periods, respectively. Figure 5 shows five pressure levels between about 40 km and 80 km. It is seen from Fig. 5a–5e that the eastward wave 1 demonstrates maximum spectral signal before the SSW onset (red curve). Westward wave 1 dominates after 10 February (black curve in Fig. 5f–5j).

This result explains that the pre-warming maximum of the wave 1 amplitude at 40–60 km (Z1 in Fig. 3a) was formed by the eastward component of $m = 1$, which is also present in the lower stratosphere (Fig. 4). At the 60–80 km altitude range, Z1 maximum in the warming and post-warming periods (Fig. 3a) was caused by the westward component of $m = -1$. Transition from eastward to westward propagated wave 1 is seen also from the wave number spectra in Fig. 5k–5o ($m = 1$ dominates) and Fig. 5p–5t ($m = -1$ dominates), respectively. Note that, if the short and long periods (<5 days and >5 days) are present in the first interval, then the periods longer than 10 days dominate in the second interval (Fig. 3k–3o and Fig. 3p–3t, respectively).

Preprints (www.preprints.org) | NOT PEER-REVIEWED | Posted: 2 February 2021 doi:10.20944/preprints202102.0093.v1

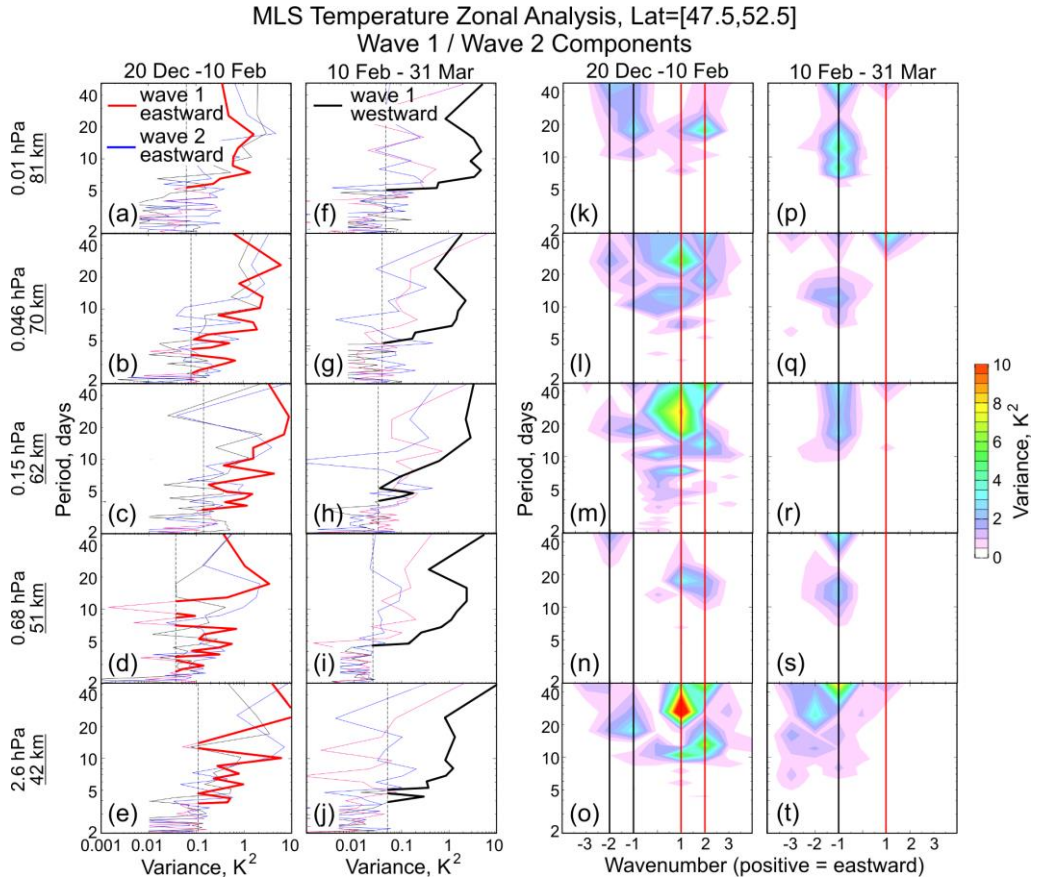

Figure 5. The spectral analysis of the zonal temperature anomalies as in Fig. 2 (middle and right) but for the upper stratosphere–mesosphere: (**a**–**e**, **k**–**o**) before and (**f**–**j**, **p**–**t**) after the SSW start on 10 February 2018. Red and black lines indicate the eastward and westward propagating wave numbers, respectively. Bold curves to the right of dashed line in (**a**–**j**) and spectra in (k–t) show the wave number variance exceeding the 95% confidence limit.

Thus, only the longest (m = –1) and long-periodic (tens of days) waves dominated in the mid-latitude mesosphere after the zonal wind reversal in the SSW 2018 (Fig. 5p–5t).

It becomes clear also that the pre-warming maximum of the wave 2 amplitude in the stratosphere–lower mesosphere (Z2 in Fig. 3b) appeared due to the eastward component contribution (m = 2 in Fig. 5k–5o), which disappeared later (no spectral signal at m = 2 in Fig. 5p–5t).

3.3. Wavelet analysis of mesospheric CO variability

In addition to zonal wind, temperature and geopotential height, we examined the wave spectra in the mesospheric CO variability using the MWR and MLS data processed with the wavelet transform (Fig. 6).

Wavelet analysis reveals the changes in the periodic oscillations with time [30]. Pay attention to the mesospheric spectral peaks of the eastward wave 1 in the pre-warming period (5–30 days at m = 1 in Fig. 5k–5m). They appear as a sequence of increasing periods in the CO variations during January until the SSW onset from both the MWR and MLS data (Fig. 6a and 6d). Westward wave 1 dominated after the zonal wind reversal (10–30 days at m = –1 in Fig. 5p–5r) exhibits slowly increasing periods at the 20–30-days (early February–March in Fig. 6a and 6d). The wavelet power spectra in Fig. 6b and 6e confirm that a statistically significant signal falling into the cone of influence is observed on 20–30-day periods during the SSW only.

Preprints (www.preprints.org) | NOT PEER-REVIEWED | Posted: 2 February 2021 doi:10.20944/preprints202102.0093.v1

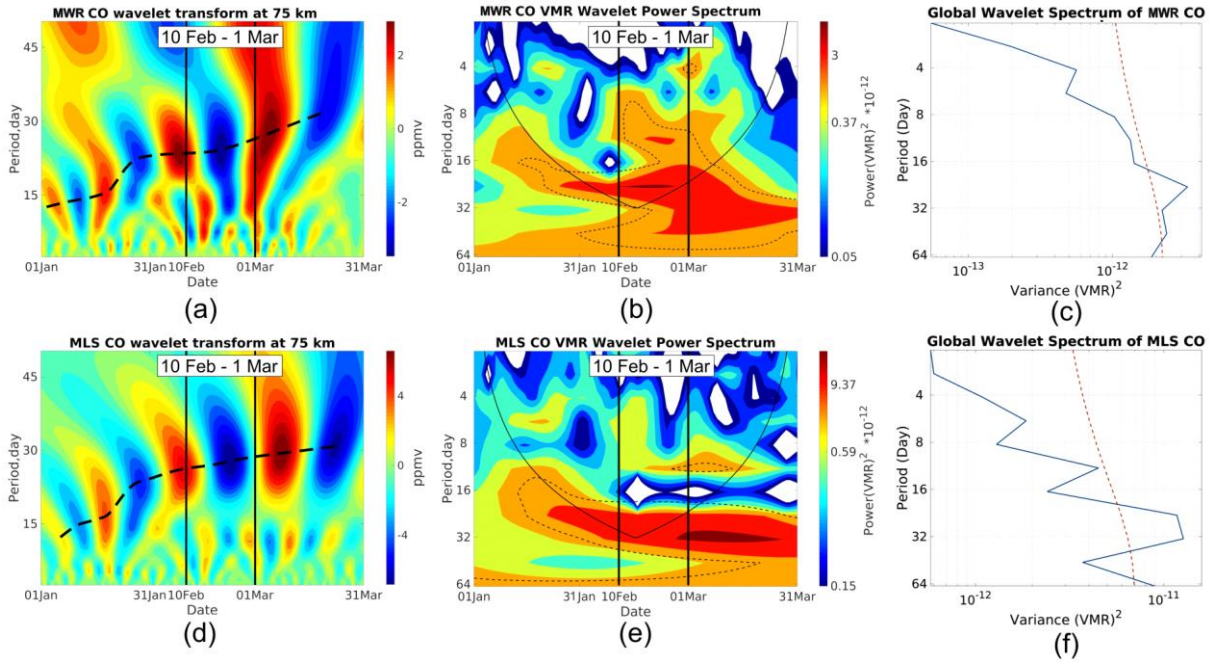

Figure 6. The wavelet transform with the real part of the Morlet function for CO from (**a**) MWR data and (**d**) MLS data at 75 km altitude for January 01 – March 31, 2018; (**b**), (**e**) Power spectrum of the wavelet transform shown in (**a**), (**d**) and the solid curve is the cone of influence, within which the spectrum is not significantly influenced by boundary effects. (**c**), (**f**) Global wavelet spectrum for (**b**), (**e**). Dashed contour in (**b**), (**e**) and dashed curve in (**c**), (**f**) show the 95% confidence level with the white-noise background spectrum.

As shown in Fig. 6, before the occurrence of SSW, the main periods of CO content at 75 km was ~15–20 days (Fig. 6 a, b, d and e), and there was also a short period of ~5 days fluctuations. The latter is statistically insignificant in the wavelet transform (Fig. 6b and e), but is significant in the spectra of the MLS temperature variations in the mesosphere (Fig. 5a–c). After the SSW onset, the smaller period of ~10 days occurred (Fig. 6b and e), but the large periods of 20 to 35 days were dominant, which were contributed mainly by westward wave 1 (m = –1 in Fig. 5p–q). After the end of SSW, the statistically significant periods become larger, although outside the cone of influence (Fig. 6d and e), which means that the change of CO approaches quasi-stable.

Wave 2 played important role in the SSW 2018 and caused the stratospheric polar vortex split (Rao et al., 2018; Wang et al., 2019; Butler et al., 2020). As seen form (Fig. 4g–4i, m =2), wave 2 tends to be quasi-stationary in the pre-warming stratosphere.

The eastward traveling wave 2 was observed in the pre-warming mesosphere (15–20-day periods at m = 2 in Fig. 5r–5l) and no wave 2 signal appears in both the stratosphere and mesosphere after the zonal wind reversal, as noted above (Fig. 3b and m = 2 in Fig 5p–5t). This is evidence that the quasi-stationary wave 2 (Fig. 4g–4i, m =2) was responsible for the stratospheric polar vortex split in February 2018.

4. Discussion

The impacts of the polar stratosphere dynamics during the SSW 2018 on the mid-latitude stratosphere and mesosphere were analyzed. It was found that abrupt changes in the upward propagation of planetary waves and zonal migration of wave-induced anomalies, as well as in the spectrum and periodicity of waves occurred near 50° N with the zonal wind reversal after 10 February 2018 (Figs. 1–6 in Section 3–5).

The role of the zonal wave 1 and wave 2 in the SSW preconditioning and development is known from many studies [1,12,31–34]. We have shown that wave 1 and wave 2 dominated in the mid-latitude stratosphere and lower mesosphere in the pre-warming period and at the SSW onset (Fig. 3) and that they were quasi-stationary in their proper-

Preprints (www.preprints.org) | NOT PEER-REVIEWED | Posted: 2 February 2021 doi:10.20944/preprints202102.0093.v1

ties (m = –1 and m = 2 in Fig. 4g–4i). It is quasi-stationary wave 2 that was responsible for the splitting of the polar vortex in SSW 2018, in consistency with other studies (e.g. Ma et al., [14] 2020), and the manifestation of this large-scale polar process was observed in the midlatitudes. This is not surprising, since from the mid-February, zonal wind reversal to the easterlies expanded into the extratropics forming the stratospheric easterly layer between the polar and tropical latitudes (Fig. 1c–1e).

Zonal wind reversal had a dramatic effect on the planetary wave structure. Upward displacement of the westerly layer into the mesosphere (Fig. 1c–1e) associated with the elevated stratopause [33] was accompanied by similar change in vertical profile of wave 1 (Fig. 3a). Wave 1 had the two components in the pre-warming stratosphere: eastward migrating (black dashed lines in Fig. 4c and m = 1 in Fig. 4g–4i) and slowly westward migrating quasi-stationary (black–white dashed line in Fig. 4a–4c and m = –1 in Fig. 4g–4i). In the mesosphere, wave 1 was replaced from eastward migrating to westward migrating with the wind reversal (m = 1 and m = –1 in Fig. 5k–5m and 5p–5r, respectively). This change is clearly indicated with dashed lines in Fig. 2a and 2b. Note that such a change in zonal migration of wave-induced mesospheric anomalies, as far as we know, has been illustrated for the first time.

Easterly zonal flow in the stratosphere, as noted in Section 3, prevents upward planetary wave propagation according Charney and Drazin [4]. Therefore, the appearance of the westward wave 1 in the mesosphere cannot be caused by tropospheric sources. The simulations made by Limpasuvan et al. [33] show that the westward propagating planetary wave 1 forcing dominates in the polar mesosphere with the SSW onset. The presence of in situ forced planetary waves around the SSW onset due to the eastward (or westerly) jet instability in the polar mesosphere was discussed in [33,35]. Limpasuvan et al. [33] have shown that, around the SSW onset, spectral power of the westward wave 1 increases in the polar mesosphere (their Fig. 10b). Chandran et al. [35] noted that the reversal of the stratospheric jet at high latitudes in the winter hemisphere leads to conditions conducive to the generation of short period waves via instability of the background zonal wind field. Wavelet power spectra show statistically significant signal in the mesospheric CO variability at the 20–30-day periods (Fig. 6). However, if we take the westward wave 1 spectral component, it has maximum spectral power during the SSW 2018 event at the 10–20-day periods (Fig. 5f, 5g, 5p and 5q). The shorter wave 1 periods 5–10 days was observed in the pre-warming mesosphere (Fig. 5k–5m). Our results on westward wave 1 suggest that some kind of westerly instability in the midlatitude mesosphere is possible. This possibility needs to be examined in the simulations in the further analysis.

5. Conclusions

This study presents the changes in the mid-latitude planetary wave spectra associated with the SSW 2018 and their altitudinal dependence. The main conclusion is that the abrupt changes in the wave properties are associated with zonal wind reversal in the stratosphere at the SSW onset. These consistent changes are observed in: (1) the penetration of zonal waves 1 and wave 2 from the troposphere into the stratosphere and mesosphere with likely generation of westward wave 1 in the mesosphere, (2) the direction of the zonal anomaly migration in the mesosphere from eastward to westward, (3) the wave spectrum with the disappearance of wave 1 in the stratosphere and wave 2 in the entire altitude range (10–90 km), and (4) the mesospheric wave 1 periods 10–20 days with disappearance of the shorter 5–10-day periods observed in the pre-warming mesosphere. It should be noted that the mesospheric CO variability in the Kharkiv region show the maximum spectral power at 20–30-day periods from both ground-based (MWR data) and satellite (MLS data) observations.

It is interesting that the two wave 1 components are simultaneously present in the pre-warming stratosphere: eastward traveling and quasi-stationary (slowly migrating westward). Generally, the results are in agreement with other studies and confirm that (i)

quasi-stationary wave 2 is responsible for the stratospheric polar vortex split in February 2018 and (ii) westward wave 1 dominates in the post-warming mesosphere.

It is known from previous works that the westward wave 1 increases in the mesosphere during the SSW may be caused by an unstable westerly polar jet. This possible instability needs to be further explored in the simulations considering the mid-latitude mesosphere conditions during the SSW.

Author Contributions: Conceptualization, A.K., O.E. and G.M.; methodology, O.E., A.K. and Y.W.; data acquisition, A.K., Y.W., V.S., and O.A.; software, A.G., Y.W. and A.K.; validation, A.G., A.K., O.E. and G.M.; investigation, O.E., G.M. and A.K.; writing—original draft preparation, A.G., O.E., Y.W., and G.M.; writing—review and editing, A.G., V.S., O.E., A.K. and G.M.; visualization, O.E., A.G., Y.W. and O.I.; supervision, G.M. and A.K.; project administration, G.M., V.S. and W.H. Each author contributed to the interpretation and discussion of the results and edited the manuscript. All authors have read and agreed to the published version of the manuscript.

Funding: This research received no external funding.

Data Availability Statement: The MWR data presented in this study are available on request from the author V.S.

Acknowledgments: This work was supported in part by the Institute of Radio Astronomy of the National Academy of Sciences of Ukraine; by Taras Shevchenko National University of Kyiv, projects 19BF051-08 and 20BF051-02; by the College of Physics, International Center of Future Science, Jilin University, China. This work contributed to the National Antarctic Scientific Center of Ukraine research objectives, and contributed to Project 4293 of the Australian Antarctic Program. The microwave radiometer data were processed using the ARTS and Qpack software packages (http://www.radiativetransfer.org/). The Aura Microwave Limb Sounder (MLS) measurements of zonal wind, geopotential height, air temperature and CO were obtained from https://mls.jpl.nasa.gov/data/readers.php.

Conflicts of Interest: The authors declare no conflict of interest.

References

1. Matsuno, T. A dynamical model of the stratospheric sudden warming. *J. Atmos. Sci*. **1971**, *28*, 1479–1494, doi:10.1175/1520-0469(1971)028<1479:ADMOTS>2.0.CO;2.
2. Waugh. D.W.; Polvani L.M. Stratospheric polar vortices. In: The Stratosphere: Dynamics, Transport, and Chemistry, Geophysical Monograph Series, **2010**, *190*, 43–57, doi:10.1002/9781118666630.ch3.
3. Kozubek, M.; Krizan, P.; Lastovicka, J. Northern Hemisphere stratospheric winds in higher midlatitudes: longitudinal distribution and long-term trends. *Atmos. Chem. Phys*. **2015**, *15*, 2203–2213, doi:10.5194/acp-15-2203-2015.
4. Charney J.G.; Drazin P.G. Propagation of planetary-scale disturbances from the lower into the upper atmosphere. *J. Geophys. Res.* **1961**, *66*, 83–109, doi:10.1029/JZ066i001p00083.
5. Dickinson, R.E. Planetary Rossby waves propagating vertically through weak westerly wind wave guides, *J. Atmos. Sci.* **1968**, *25*, 984–1002, doi:10.1175/1520-0469(1968)025<0984:PRWPVT>2.0.CO;2.
6. Matsuno, T. Vertical propagation of stationary planetary waves in the winter Northern Hemisphere. *J. Atmos. Sci*. **1970**, *27*, 871–883, doi:10.1175/1520-0469(1970)027<0871:VPOSPW>2.0.CO;2.
7. Plumb, R.A. Planetary Waves and the Extratropical Winter Stratosphere. In: The Stratosphere: Dynamics, Transport, and Chemistry Geophysical Monograph Series, **2010**, 190, 23–41, doi:10.1002/9781118666630.ch2.
8. Domeisen, D.I.V.; Martius, O.; Jiménez-Esteve, B. Rossby wave propagation into the Northern Hemisphere stratosphere: The role of zonal phase speed. Geoph. Res. Lett. **2018**, *45*, 2064–2071, doi:10.1002/2017GL076886.
9. Butler, A.; Seidel, D.; Hardiman, S.; Butchart, N.; Birner, T.; Match, A. Defining sudden stratospheric warmings. *Bull. Am. Meteorol. Soc.* **2015**, *96*, 1913–1978, doi:10.1175/BAMS-D-13-00173.1.
10. Butler, A.H.; Sjoberg, J.P.; Seidel, D.J.; Rosenlof, K.H. A sudden stratospheric warming compendium. *Earth Syst. Sci. Data* **2017**, *9*, 63–76, doi:10.5194/essd-9-63-2017.
11. Butler, A.H.; Gerber, E.P. Optimizing the definition of a Sudden Stratospheric Warming. *J. Clim.* **2018**, *31*, 2337–2344, doi:10.1175/JCLI-D-17-0648.1.
12. Wang, Y.; Shulga, V.; Milinevsky, G.; Patoka, A.; Evtushevsky, O.; Klekociuk, A.; Han, W.; Grytsai, A.; Shulga, D.; Myshenko, V.; Antyufeyev, O. Winter 2018 major sudden stratospheric warming impact on midlatitude mesosphere from microwave radiometer measurements. *Atmos. Chem. Phys*. **2019**, *19*, 10303–10317, doi:10.5194/acp-19-10303-2019.
13. Butler, A.H.; Lawrence, Z.D.; Lee, S.H.; Lillo, S.P.; Long, C.S. Differences between the 2018 and 2019 stratospheric polar vortex split events. *Q. J. R. Meteorol. Soc.* **2020,** 1–19, doi:10.1002/qj.3858.

14. Ma, Z.; Gong, Y.; Zhang, S.D.; Luo, J.H.; Zhou, Q.H.; Huang, C.M.; Huang, K.M. Comparison of stratospheric evolution during the major sudden stratospheric warming events in 2018 and 2019. *Earth Planet. Phys.* **2020**, *4*, 493–503, doi:10.26464/epp2020044.
15. Schoeberl, M.R. Stratospheric warmings: Observations and theory. *Rev. Geophys.* **1978**, *16*, 521–538, doi:10.1029/RG016i004p00521.
16. Esler, J.G.; Polvani, L.M.; Scott R.K. The Antarctic stratospheric sudden warming of 2002: A self-tuned resonance? *Geophys. Res. Lett*. **2006**, *33*, L12804, doi:10.1029/2006GL026034.
17. Cao, C.; Chen, Y.-H.; Rao, J.; Liu, S.-M.; Li, S.-Y.; Ma, M.-H.; Wang, Y.-B. Statistical Characteristics of Major Sudden Stratospheric Warming Events in CESM1-WACCM: A Comparison with the JRA55 and NCEP/NCAR Reanalyses. *Atmosphere* **2019**, *10*, 519. https://doi.org/10.3390/atmos10090519.
18. Kuttippurath, J.; Nikulin, G. A comparative study of the major sudden stratospheric warmings in the Arctic winters 2003/2004–2009/2010. *Atmos. Chem. Phys*. **2012**, *12*, 8115–8129, doi:10.5194/acp-12-8115-2012.
19. Varotsos, C. The extraordinary events of the major, sudden stratospheric warming, the diminutive Antarctic ozone hole, and its split in 2002. *Environ. Sci. Pollut. Res.* **2004**, *11*, 405, doi:10.1007/BF02979661.
20. Nishii, K.; Nakamura, H. Tropospheric influence on the diminished Antarctic ozone hole in September 2002. *Geophys. Res. Lett*. **2004**, *31*, doi:10.1029/2004GL019532.
21. Lim, E.-P.; Hendon, H.H.; Butler, A.H.; Garreaud, R.D.; Polichtchouk, I.; Shepherd, T.G.; Scaife, A.; Comer, R.; Coy, L.; Newman, P.A.; et al. The 2019 Antarctic sudden stratospheric warming. *SPARC15 Newsletter* **2020**, *54*, 10–13, http://www.sparc-climate.org/publications/newsletter.
22. Milinevsky, G.; Evtushevsky, O.; Klekociuk, A.R.; Wang, Y.; Grytsai, A.; Shulga, V.; Ivaniha, O. Early Indications of Anomalous Behavior in the 2019 Spring Ozone Hole over Antarctica. *Int. J. Remote Sens*. **2020**, 41, 7530–7540, doi:10.1080/2150704X.2020.1763497.
23. Gray, L.J.; Brown, M.J.; Knight, J.; Andrews, M.; Lu, H.; O'Reilly, C.; Anstey, J. Forecasting extreme stratospheric polar vortex events. *Nat. Commun.* **2020**, *11*, 4630, doi:10.1038/s41467-020-18299-7.
24. Rüfenacht, R.; Kämpfer, N.; Murk, A. First middle-atmospheric zonal wind profile measurements with a new ground-based microwave Doppler-spectroradiometer. *Atmos. Meas. Tech*. **2012**, *5*, 2647–2659, doi:10.5194/amt-5-2647-2012.
25. Schwartz, M.J.; Lambert, A.; Manney, G.L.; Read, W.G.; Livesey, N.J.; Froidevaux, L.; Ao, C.O.; Bernath, P.F.; Boone, C.D.; Cofield, R.E.; et al. Validation of the Aura Microwave Limb Sounder temperature and geopotential height measurements. *J. Geophys. Res*. **2008**, *113*, D15S11, doi:10.1029/2007JD008783.
26. Xu, X.; Manson, A.H.; Meek, C.E.; Chshyolkova, T.; Drummond, J.R.; Hall, C.M.; Riggin, D.M.; Hibbins, R.E. Vertical and interhemispheric links in the stratosphere-mesosphere as revealed by the day-to-day variability of Aura-MLS temperature data. *Ann. Geophys*. **2009**, *27*, 3387–3409, doi:10.5194/angeo-27-3387-2009.
27. Livesey, N.J.; Read, W.G.; Wagner, P.A.; Froidevaux, L.; Lambert, A.; Manney, G. L.; Millán Valle, L.F.; Pumphrey, H.C.; Santee, M.L.; Schwartz, M.J.; et al. EOS MLS version 4.2x–3.1 Level 2 data quality and description document, Tech. rep., Jet Propulsion Laboratory, available from https://mls.jpl.nasa.gov/data/v4-2_data_quality_document.pdf, 2018.
28. MLS: Microwave Limb Sounder EOS MLS Data Readers. Available online: https://mls.jpl.nasa.gov/data/readers.php (accessed on 15 January 2021).
29. Fleming, E.L.; Chandra, S.; Barnett, J.J.; Corney, M. Zonal mean temperature, pressure, zonal wind, and geopotential height as functions of latitude. *Adv. Space Res*. **1990**, *10*, 11–59, doi:10.1016/0273-1177(90)90386-E.
30. Torrence, C.; Compo, G.P. A practical guide to wavelet analysis. *Bull. Amer. Meteorol. Soc*. **1998**, *79*, 61–78. doi:10.1175/1520-0477(1998)079<0061:APGTWA>2.0.CO;2.
31. Manney, G.L.; Schwartz, M.J.; Krüger, K.; Santee, M.L.; Pawson, S.; Lee, J.N.; Daffer, W.H.; Fuller, R.A.; Livesey, N.J. Aura Microwave Limb Sounder observations of dynamics and transport during the record-breaking 2009 Arctic stratospheric major warming. *Geophys. Res. Lett*. **2009**, *36*, L12815, doi:10.1029/2009GL038586.
32. Yuan, T.; Thurairajah, B.; She, C.Y.; Chandran, A.; Collins, R.L.; Krueger, D.A. Wind and temperature response of midlatitude mesopause region to the 2009 Sudden Stratospheric Warming. *J. Geophys. Res*. **2012**, *117*, D09114, doi:10.1029/2011JD017142.
33. Limpasuvan, V.; Orsolini, Y.J.; Chandran, A.; Garcia, R.R.; Smith, A.K. On the composite response of the MLT to major sudden stratospheric warming events with elevated stratopause. *J. Geophys. Res. Atmos*. **2016**, *121*, 4518–4537, doi:10.1002/2015JD024401.
34. Rao, J.; Ren, R.; Chen, H.; Yu, Y.; Zhou, Y. The stratospheric sudden warming event in February 2018 and its prediction by a climate system model. *J. Geophys. Res.-Atmos*. **2018**, *123*, 13332–13345, doi:10.1029/2018JD028908.
35. Chandran, A.; Garcia, R.R.; Collins, R.L.; Chang, L.C. Secondary planetary waves in the middle and upper atmosphere following the stratospheric sudden warming event of January 2012. *Geophys. Res. Lett*. **2013**, *40*, 1861–1867, doi:10.1002/grl.50373.